Published in final edited form as:
J Biomed Mater Res A. 2010 November ; 95(2): 333–340. doi:10.1002/jbm.a.32840.

The Controlled Induction of Distributed Microdeformation in Wounded Tissue via a Microchamber Array Dressing

Bartholomew J. Kane, M.D., Ph.D.[1,*], **George Younan, M.D.**[2,*], **Douglas Helm, M.D.**[2], **Pouya Dastouri, M.D.**[2], **Harrison Prentice-Mott, B.A.**[3], **Daniel Irimia, M.D., Ph.D.**[4], **Rodney K. Chan, M.D.**[2], **Mehmet Toner, Ph.D.**[4], and **Dennis P. Orgill, M.D., Ph.D.**[2]

[1] Division of Pediatric Surgery, Department of Surgery, University of Virginia Health System, Charlottesville, VA 22908

[2] Brigham and Women's Hospital, Harvard Medical School, Division of Plastic Surgery, Boston, MA 02115

[3] BioMEMS Resource Center, Center for Engineering in Medicine, Massachusetts General Hospital, Boston, MA

[4] Shriner's Hospital for Children, Boston, MA

Abstract

Mechanical stimuli are known to play an important role in determining the structure and function of living cells and tissues. Recent studies have highlighted the role of mechanical signals in mammalian dermal wound healing. However, the biological link between mechanical stimulation of wounded tissue and the subsequent cellular response has not been fully determined. The capacity for researchers to study this link is partially limited by the lack of instrumentation capable of applying controlled mechanical stimuli to wounded tissue. The studies outlined here tested the hypothesis that it was possible to control the magnitude of induced wound tissue deformation using a microfabricated dressing, comprised of an array of open-faced, hexagonally-shaped microchambers rendered in a patch of silicone rubber. By connecting the dressing to a single vacuum source, the underlying wounded tissue was drawn up into each of the microchambers, thereby inducing tissue deformation. For these studies, the dressings were applied to full thickness murine dermal wounds with 200 mmHg vacuum for 12 hours. The studies demonstrated that the dressing was capable of inducing wound tissue deformation with values ranging from 11 to 29 %. Through statistical analysis, the magnitude of the induced deformation was shown to be a function of both microchamber height and width. These results demonstrated that the dressing was capable of controlling the amount of deformation imparted in the underlying tissue. By allowing the application of mechanical stimulation with varying intensity, such a dressing will enable the performance of sophisticated mechanobiology studies in dermal wound healing.

Keywords

Microfabrication; microfluidic devices; negative-pressure wound therapy; micromechanical forces; wound healing

Corresponding Author: Dennis P. Orgill, Brigham and Women's Hospital Division of Plastic Surgery, 75 Francis Street, Boston, MA 02115, (P) 617-732-5456, (F) 617-730-2855, dorgill@partners.org.
*Authors contributed equally to this work

AUTHOR DISCLOSURE STATEMENT
No competing financial interests exist.

INTRODUCTION

Mechanical stimuli have long been recognized as an important factor in determining the structure and function of living cells and tissues.[1,2] For decades, physicians have been applying mechanical loads to living tissue in order to achieve beneficial therapeutic effects. Distraction osteogenesis is an example wherein gradual lengthening of long bones is realized by the sequential application of axial forces.[3,4] Similarly, tissue expanders allow gradual lengthening of soft tissues.[5,6] In order to better understand these clinical effects, researchers have been studying the molecular and cellular responses to mechanical stimulation with increasing intensity. The first mechanically responsive transmembrane signaling proteins was recognized over 20 years ago.[7] Several other transmembrane proteins capable of mechanical transduction have been recognized since that time.[8,9] More recently, researchers have begun to uncover the mechanisms that allow transmission of mechanical signals from the cell membrane to the nucleus. These signals are transmitted through the cytoplasm to activate gene expression in the nucleus, thereby producing phenotypic changes in the cell.[1,2,8,10,11] Several recent studies have established a direct relationship between cell stretch and cell proliferation.[12,13] In further demonstration of the link between mechanics and cell behavior, a recent study noted that changes in the stiffness of the substrate upon which cells are supported can effect cell proliferation, migration, and differentiation.[12,14]

Just as in distraction osteogenesis and tissue expansion, mechanical stimulation has been found to have a clinical effect on dermal wound healing. Traction-assisted dermatogenesis has been documented as a low cost and effective method that enables the reconstruction of complex dermal wounds.[15] Negative pressure wound therapy (NPWT), as typified by the Vacuum-Assisted Closure (VAC) device, is another form of mechanical therapy that is widely used in the treatment of complex wounds.[16–19] A known effect of NPWT is the induction of microdeformation at the surface of wounded tissue. Researchers have hypothesized that this microdeformation promotes cell proliferation through the activation of mechanotransduction pathways.[20–22] Recent studies have demonstrated a correlation between tissue microdeformations induced by NPWT and the activation of both cell proliferation and angiogenesis in murine dermal wounds.[18,19,21,22] But, the mechanisms through which cellular proliferation and angiogenesis are triggered have yet to be determined.

The capacity for wound healing researchers to study the link between mechanical stimulation and biological response is limited by the lack of instrumentation capable of stimulating the tissue in an appropriate manner. Although devices such as the VAC are able to induce sustained microdeformation on the surface of wounded tissue, the magnitude of the induced deformation is not easily controlled or quantified.[23,24] With the studies outlined in this article, the authors tested the hypothesis that it was possible to control the magnitude of induced deformation in wounded tissue by using a microdressing system. Note that this hypothesis was not concerned with the effects of this microdeformation on active wound healing or wound healing parameters. This initial study was exclusively focused on the controllability of microdeformation in wounded tissue and was not an attempt to explore the wound healing benefits of the dressing.

To test this hypothesis, microfabrication techniques were used to develop a dressing capable of inducing controlled and distributed tissue microdeformation. Advances in microfabrication technology over the last several decades have expanded our capacity to manipulate cells and tissue on the microscale.[25–27] Though these techniques were originally developed for the construction of integrated circuits, they are now commonly used for the development of mechanical, electrical, fluidic, biological, and chemical microstructures. In

particular, microfabricated fluidic systems are increasingly being deployed in biomedical devices and analytical systems with diagnostic, therapeutic, and basic science research endpoints.[28] Microfluidic systems enable the controlled manipulation of small volumes of fluids in a parallel manner, thereby maximizing throughput.

MATERIALS AND METHODS

Microchamber Array Design

The primary goal of the dressing design was to achieve a uniform distribution of tissue deformation in the surface of wounded tissue. The approach taken to achieve this goal was to construct a flexible array of open faced microchambers, each capable of transmitting a sub-atmospheric pressure to the underlying wound tissue. With the application of this sub-atmospheric pressure, wound tissue was drawn into each microchamber, thereby inducing tissue deformation. The microchamber array dressing (μCAD), shown schematically in Figure 1, was constructed by bonding together two layers of patterned polydimethylsiloxane (PDMS) silicon rubber. The bottom surface of the dressing was comprised of open-faced hexagonally shaped microchambers in an array configuration. The choice of a hexagon for the microchambers was arbitrary, but did serve to mimic the circular geometry of the open cell foam material used for negative pressure wound therapy (NPWT). Within any single array, the microchambers were all the same size. But, the size of the microchambers between dressings varied between 200, 500, and 1000 μm in width and 100, 200, and 300 μm in height, yielding nine unique microchamber sizes. The top of each microchamber was equipped with a fenestration to allow connection to a vacuum distribution microchannel contained within the second layer of the dressing. The channel in the second layer was 100 μm high and was supported by distributed 100 μm diameter round pillars to maintain patency.

The total thickness of the bottom microchamber layer was controlled to values of 200, 300, and 400 μm. The total thickness of the second vacuum distribution layer was not specifically controlled and ranged between 1.7 – 2.3 mm. The two layers together resulted in a dressing with thicknesses between 1.9 – 2.7 mm. A single fenestration was formed through the top of the second layer to allow the insertion of tubing for connection to a vacuum source.

Dressing Fabrication

Microfabrication techniques were chosen to develop this dressing because they enabled the construction of a broad range of microchamber sizes, from tens of microns to millimeters. In addition, microfabrication techniques allowed the construction of a network of microchannels to distribute sub atmospheric pressure to the microchambers. The arrays were fabricated in a three phase process.

In the first phase of construction, two molds were made using photolithographic techniques. Each mold corresponded to a single layer of the two-layer dressing. The geometries of the molds were rendered on the surface of a 4 inch silicon wafer in an epoxy based photoresist (NANO™ SU-8 50, MicroChem, Newton, MA) using microphotolithography. This was done by spinning on a uniform layer of SU-8 with a goal thickness corresponding to the desired structure. The SU-8 was then baked at 65 °C for 10 min and 100 °C for 30 min. At this point, the photoresist was patterned using a contact mask aligner (2001 CT mask aligner with Ultra-Sense™ power supply, Quintel Corporation, San Jose, CA, exposure time = 40 sec, power = 16 mW/cm^2) and a 10μm resolution photomask (Advanced Reproductions Corporation, North Andover, MA). A post-exposure bake was then performed on a hot plate at 65 °C for 3 min and 95 °C for 10 min.

Both the vacuum distribution layer and the hexagonal microchambers were formed using this process. In order to realize the holes at the top of each microchamber, these steps were repeated to pattern a second layer of SU-8 on top of the hexagonal microchamber geometries. The patterns were then developed by immersion in developer (Thinner P Microposit™ thinner, Shipley Company, Marlborough, MA) for 30 min before being subjected to a final bake on a hot plate at 65 °C for 3 min and 95 °C for 10 min. The pattern thicknesses of both molds were measured via microscope outfitted with a vertical position focus sensor (Olympus BX60 Microscope, Kramer Scientific Corporation, Amesbury, MA).

Once the two molds were completed, the second phase of the fabrication process was initiated. At that time, liquid polydimethylsiloxane (SYLGARD® 184 Silicone Elastomer, Dow Corning Corporation, Midland, MI) was prepared by mixing a liquid base and a liquid curing agent with a weight ratio of 10:1. This liquid mixture was then poured over the bottom microchamber array mold before a Mylar film was placed on top of both the mold and the PDMS. The wafer and the Mylar film were then placed between two aluminum plates before a moderate amount of force was applied to the two plates with a standard c-clamp. This force served to both evacuate the excess liquid PDMS from the mold cavity and to create via holes at the top of each microchamber in the array. The PDMS was allowed to cure for 12 hrs at room temperature before it was removed from the press apparatus and placed into a 60 °C oven for 4 hrs to complete the curing process.

The vacuum distribution layer was formed similarly by pouring the liquid PDMS over the corresponding mold before placed it into a 60 °C oven for 4 hrs to complete the curing process. In this case, the mold and liquid PDMS was not compressed with an overlying Mylar film. The target thickness of this layer was 2 millimeters.

In order to produce a bond between the vacuum distribution layer and the microchamber layer, both underwent a brief plasma etch (PX-250, March Instruments Incorporated, Concord, CA, power = 200 mW/cm^2, oxygen flow rate = 2 %, time = 30 sec). Once the plasma step was completed, the PDMS layers were hand aligned relative to each other under a long working distance microscope (Combizoon-400 Microscope, Kramer Scientific Corporation, Amesbury, MA). Once alignment was obtained and the two layers were brought into contact, they were placed on a hot plate at 65 °C for 10 minutes to potentiate bonding.

To allow introduction of sub-atmospheric pressure into the array, an opening was cut into the top surface of the vacuum distribution layer using a 30 gage leur plug. Tygon tubing with an inner diameter of 0.32 mm and an outer diameter of 0.45 mm was then press-fit into the resulting hole. A completed array is shown in Figure 2.

Animals, Tissue Models, and Study Groups

To quantify the microdeformation induced by the μCAD, the dressing was studied using a murine wound model. Sixteen heterozygous 8 – 12 week old, Lep/r-db/+ male mice, (C57BL/KsJLepr-db) were used under an approved animal protocol by the Harvard Experimental Animal Committee in an Association for Assessment and Accreditation of Laboratory Animal Care (AAALAC) accredited facility. One day prior to surgery, the dorsal hair of the animal was clipped and a depilatory solution (Nair R, Church and Dwight Company, Inc., Princeton, NJ) was applied to the underlying skin. Minutes prior to surgery, the animals were anesthetized with 60 mg/kg Nembutal (Pentobarbital). Following disinfection with a 70% alcohol solution, 1 x 1 cm square of skin and panniculus carnosus was excised from the dorsum of the animals. The animals were then sacrificed and the wound area with the 0.5 cm surrounding skin and underlying tissue was harvested. The dressing was applied to the tissue, taking care to ensure that the microchambers were

positioned face-down relative to the wound. Sub-atmospheric pressure which was supplied to the dressing via the plastic tubing; was generated by linking the regular laboratory suction port to a suction regulator (Puritan Bennett™, Covidien, Boulder, CO). The value of the sub-atmospheric pressure was set at 200 mmHg, representing the upper end of the range of magnitudes used for NPWT in the clinical setting. The array was fixed onto the tissue using a Tegaderm™ tape (3M Healthcare, St. Paul, MN).

It should again be noted here that the scope of the hypothesis tested in this article was intentionally limited such that a live animal study was not necessary. The study outlined in this article tested only the hypothesis that it was possible to control the magnitude of induced wound tissue deformation through the use of the novel dressing system. It was not an attempt to explore the wound healing benefits of the dressing. For this reason, the deformation studies were performed using full thickness wounds in dermal tissue that had been explanted from sacrificed animals.

Nine unique microchamber geometries (width = 200, 500, and 1000 μm, height = 100, 200, or 300 μm) were used in these studies. Each of these was applied to four wounds for 12 hours with 200 mmHg suction. A positive control was achieved by applying the same sized microchamber dressings to four excisional wounds without sub-atmospheric pressure. A negative control was achieved by covering four wounds with Tegaderm only. After the application of the dressing, the tissues were fixed in 10 % neutral-buffered formalin solution for 24 hours with the μCAD left *in situ* and transferred to a 70 % ethanol solution at room temperature until the tissue was embedded in paraffin prior to histological sectioning.

Tissue Deformation Determination

To quantify the microdeformation induced in the wounded tissue by the microchamber dressing, central wound sections were stained with Hematoxylin and Eosin (H&E). The undeformed and deformed wound surface lengths were then measured using serial 10x histological micrographs. Care was taken to ensure that the sections were taken in line with the axis of the rows of the array and through the center of a series of microchambers. Measurements were made using digital planimetry (Image J 1.42, National Institutes of Health, Bethesda, MD). The magnitude of the induced deformation was determined by subtracting the original, undeformed length of the wound surface from the deformed length and dividing that quantity by the undeformed wound length. An example of the geometries used to make these calculations is illustrated in Figure 3.

Statistical Analysis

All values expressed in the text and figures were calculated as averages with standard deviations. In order to determine which of the microchamber geometries significantly impacted the magnitude of the induced tissue deformation, an analysis of variance study was performed. ANOVA was used to evaluate significant differences between the deformation data from each of the nine groups corresponding to each of the nine distinct microchamber geometries. Specifically, a post-hock analysis using the Tukey's Honestly Significant Difference Test (HSD) was used to evaluate each of the nine means (SPSS Statistics, SPSS Inc., Chicago, IL). The HSD test was used to determine if each mean value was significantly different from the remaining eight means. The p-value indicating statistical significance was set at 0.05.

RESULTS

Microchamber Array Material and Function

Microscopic inspection of the individual microfabricated dressings demonstrated a high degree of uniformity of the microchambers within single arrays and between arrays. The top panel of Figure 4 shows representative 4x stereomicroscopic images of three dressings with chamber height of 200 μm and variable widths, including 200, 500, and 1000 μm. The bottom panel in Figure 4 shows the tissue deformation that was induced by these microchamber dressings when they were applied to full thickness murine dermis with a vacuum value of 200 mmHg for 2 hrs. These images demonstrate that polydimethylsiloxane (PDMS) had a high enough modulus of elasticity to induce deformation and leave residual imprints of the microchambers in the tissue. No material degradation, staining, or plastic deformation was observed in any array used for the studies described in this article. In addition, the dressings were able to conform to soft tissue irregularities in order to effectively transmit sub-atmospheric pressure to the underlying wounded tissue. When the dressing was immersed in distilled water and attached to a 200 mmHg vacuum via a 15 cm length of Tygon tubing with an inner diameter of 0.32 mm, the average flow rate was measured at 0.50 ml/min/cm^2 (σ = 0.03 ml/min/cm^2).

Induced Tissue Deformation

Following application of the dressings to a full thickness murine dermal wound with 200 mmHg of sub-atmospheric pressure for 12 hours, microdeformations were noted for all microchamber sizes. Figure 5 shows representative micrographs of the H&E staining following the application the microfabricated dressing and subsequent tissue fixation and sectioning. This figure demonstrates that residual deformation was induced in the wounded tissue for all microchamber sizes. Also demonstrated in Figure 5, the 200 μm wide microchambers appear to have produced significantly less deformation in the underlying tissue when compared to the 500 and 1000 μm microchambers.

The calculated magnitudes of the average tissue deformation for each microchamber size are plotted in Figure 6(a) and (b). A maximum microdeformation of 29.0 ± 8.7 % was induced by the μCAD device with the largest microchamber geometries, 1000 μm width x 300 μm height. The 500 mm width x 300 μm height microchambers induced a similar amount of tissue deformation, measured at 26.9 ± 10.7 %. The smallest amount of tissue deformation was induced by the 1000 μm width x 100 μm height microchambers. This value was measured at 11.1 ± 3.8 %. Evaluation of the control data indicated that neither control configuration generated substantial tissue microdeformation. The magnitude of the average tissue deformation induced by the negative control was 2.1 ± 0.2 % and that that for the positive control was 3.1 ± 0.5 %. A statistically significant difference was found when the tissue deformations induced by the control configurations were compared to those induced by each of the nine microchamber sizes ($p < 0.01$ for all comparisons).

In order to determine which of the microchamber geometries significantly impacted the magnitude of the induced tissue deformation, an analysis of variance study was performed as described in the methods section. The ANOVA analysis was used to evaluate significant differences between the deformation data from each of the nine groups corresponding to each of the nine distinct microchamber geometries. This analysis revealed that changing the microchamber size resulted in a statistically significant change in the induced tissue deformation for only two comparison groups.

When considering the group of microchambers with heights of 300 μm, there was a statistically significant 2.3 fold increase in mean tissue strain between the 200 μm wide microchambers and the 500 μm wide microchambers (11.9 ± 5.9 % vs. 26.9 ± 10.7 %, p =

0.038). Similarly, there was a statistically significant 2.4 fold increase when the mean tissue strain induced by the 200 μm wide microchambers was compared to that of the 1000 μm wide microchambers (11.9 ± 5.9 % vs. 29.0 ± 8.7 %, p = 0.012).

There was not a statistically significant difference when the mean tissue strain induced by the 500 μm wide microchambers was compared to that of the 1000 μm wide microchambers (26.9 ± 10.7 vs. 29.0 ± 8.7 %, p = 1.0). A trend of increasing induced tissue deformation with increasing microchamber width was observed for the 200 μm tall microchambers. The 500 μm wide microchamber induced 1.67 times greater tissue deformation than those that were 200 μm wide (12.0 ± 2.9 vs. 20.0 ± 5.1, p = 0.642). Similarly, the 1000 μm induced 1.87 times greater tissue deformation than those that were 200 μm wide (12.0 ± 2.9 vs. 22.5 ± 3.8, p = 0.305). But, based upon the p values, these differences were shown to be not statistically significant. No increase in tissue deformation was observed in the 100 μm tall microchambers as the width was varied between 200, 500, and 1000 μm.

When considering the group of microchambers with widths of 1000 μm, there was a statistically significant 2.7 fold increase between the mean tissue strain induced by the 100 μm tall microchambers when compared to that induced by the 300 μm width microchambers (11.1 ± 3.8 % vs. 29.0 ± 8.7 %, p = 0.008). There was a statistically insignificant 2.03 fold increase in mean tissue strain between the 100 μm tall microchambers and the 200 μm tall microchambers (22.5 ± 3.8 %, p = 0.22). Similarly, there was no statistically significant difference between the 200 and the 300 μm tall microchambers (p = 0.84).

There was no increase in induced tissue deformation with increasing height for the 200 μm wide microchambers. There was a trend of increasing deformation with increasing height for the 500 μm wide microchambers. But, this relationship was found to be statistically insignificant.

DISCUSSION

Dressing Materials, Fabrication, and Design

Microscopic inspection of the individual microfabricated dressings demonstrated a high degree of uniformity among the microchambers within a single array as well as between arrays. This helped to confirm that microphotolithography was a reliable method for fabricating the microchamber array dressings. The repeatability of the induced tissue deformation and the lack of material degradation indicated that polydimethylsiloxane was a good choice of construction material. These favorable mechanical characteristics have been demonstrated in other applications of the material.[29,30] Several favorable features of the dressing were clearly demonstrated during these studies. The dressing was easily manufacturing in a repeatable manner. In addition, it demonstrated durability and reliable system function. Verifying these functions underscored the potential of the microchamber array as an effective means to reliably induce tissue microdeformation. Such a device holds substantial potential to aid in the study of wound healing mechanobiology.

Control of Wound Tissue Deformation

The studies outlined in this article demonstrate that the microchamber array is capable of repeatedly inducing deformation in the surface of wounded tissue. These deformations were observable using stereomicroscopy and quantifiable using tissue staining and histological sectioning techniques in conjunction with digital planimetry. Using the described techniques, the dressings with 500 and 1000 μm width microchambers were shown to induce the most pronounced deformations. In comparison, the 200 μm width microchamber dressing demonstrated an attenuated tissue deformation. Further, there was not a significant difference in maximum induced strain between the 500 and the 1000 μm width dressings.

Through the inclusion of several control arms in the study, these induced microdeformations were demonstrated to be the result of microchamber action and not an artifact of the tissue fixation, sectioning, and staining processes.

The study also demonstrated that it is possible to control the magnitude of the induced microdeformation by changing the height and width of the microchambers. A statistically significant correlation between the microchamber height and the magnitude of the induced tissue deformation was observed within the 1000 μm wide microchamber arrays. A trend of increasing surface deformation with increasing microchamber height was observed for the dressings with 500 μm wide microchambers. As can be seen in Fig. 6(a), this correlation appeared to be linear for both microchamber widths. A statistically significant relationship between the width of the microchambers and the magnitude of the induced tissue deformation was observed only for those dressings that contained the 300 μm tall microchambers. A similar, but statistically insignificant trend was observed with the 200 μm tall microchambers. As can be seen in Fig. 6(b), the dependence of induced microdeformation upon the microchamber width did not appear to be linear.

The study outlined in this article tested only the hypothesis that it was possible to control the magnitude of induced wound tissue deformation through the use of the novel dressing system. The study was not an attempt to explore the wound healing benefits of the dressing. For this reason, a live animal model was not pursued. Simplifying the hypothesis in this manner enabled the execution of a relatively simple and inexpensive initial study to determine if further development of the construct was warranted.

Future Direction

The results outlined in this article demonstrate the ability of the microchamber array dressing to induce controlled microdeformation in wound tissue. Through our growing understanding of mechanobiology, we better understand the roles that cell stretch, substrate stiffness, and tissue deformation play in cell proliferation and differentiation.[12,13] Further, recent studies have demonstrated a correlation between the tissue microdeformation and the activation of both cell proliferation and angiogenesis in murine dermal wounds.[18,19,21,22] By combining these results, the hypothesis that the microdressing could serve to alter or enhance active wound healing in a live animal becomes plausible. To test that hypothesis, a study is currently being planned wherein the dressing is deployed in a living animal in order to characterize the capacity of the dressing to induce quantifiable changes in active wound healing. Distinct aspects of wound healing such as granulation tissue formation, cellular proliferation, and vascular in-growth have associated parameters that can be monitored, recorded, and analyzed. By quantifying these parameters at specified time points in the wound healing process, their response to microdeformation can be determined. Minor changes to the dressing will be needed in order to complete this study.

In other work, the dressing could be configured with a perfusion circuit to enable the distribution of fluid at surface of the wounded tissue. Such a fluidic circuit could enable the controlled delivery of cells, antibiotics, cytokines, and soluble growth factors to the wound surface. In the simplest embodiment, the flow rate in such a fluid circuit could be externally controlled with a syringe pump.

Acknowledgments

This research project was conducted with the support of a pilot grant from Harvard Catalyst, the Harvard Clinical and Translational Science Center under National Institutes of Health grant number UL1RR 025758-01 and in part by the National Institutes of Health under grant number P41 EB002503.

References

1. Janmey PA, McCulloch CA. Cell mechanics: integrating cell responses to mechanical stimuli. Annu Rev Biomed Eng. 2007; 9:1–34. [PubMed: 17461730]
2. Ingber DE. Cellular mechanotransduction: putting all the pieces together again. FASEB J. 2006; 20(7):811–27. [PubMed: 16675838]
3. Ai-Aql ZS, Alagl AS, Graves DT, Gerstenfeld LC, Einhorn TA. Molecular mechanisms controlling bone formation during fracture healing and distraction osteogenesis. J Dent Res. 2008; 87(2):107–18. [PubMed: 18218835]
4. Bouletreau PJ, Warren SM, Longaker MT. The molecular biology of distraction osteogenesis. J Craniomaxillofac Surg. 2002; 30(1):1–11. [PubMed: 12064876]
5. De Filippo RE, Atala A. Stretch and growth: the molecular and physiologic influences of tissue expansion. Plast Reconstr Surg. 2002; 109(7):2450–62. [PubMed: 12045576]
6. Takei T, Mills I, Arai K, Sumpio BE. Molecular basis for tissue expansion: clinical implications for the surgeon. Plast Reconstr Surg. 1998; 102(1):247–58. [PubMed: 9655439]
7. Martinac B, Buechner M, Delcour AH, Adler J, Kung C. Pressure-sensitive ion channel in Escherichia coli. Proc Natl Acad Sci U S A. 1987; 84(8):2297–301. [PubMed: 2436228]
8. Ingber DE. Tensegrity-based mechanosensing from macro to micro. Prog Biophys Mol Biol. 2008; 97(2–3):163–79. [PubMed: 18406455]
9. Kung C. A possible unifying principle for mechanosensation. Nature. 2005; 436(7051):647–54. [PubMed: 16079835]
10. Wang N, Tytell JD, Ingber DE. Mechanotransduction at a distance: mechanically coupling the extracellular matrix with the nucleus. Nat Rev Mol Cell Biol. 2009; 10(1):75–82. [PubMed: 19197334]
11. Ingber DE. Tensegrity and mechanotransduction. J Bodyw Mov Ther. 2008; 12(3):198–200. [PubMed: 19083675]
12. Wells RG. The role of matrix stiffness in regulating cell behavior. Hepatology. 2008; 47(4):1394–400. [PubMed: 18307210]
13. Atance J, Yost MJ, Carver W. Influence of the extracellular matrix on the regulation of cardiac fibroblast behavior by mechanical stretch. J Cell Physiol. 2004; 200(3):377–86. [PubMed: 15254965]
14. Chin MS, Lancerotto L, Helm DL, Dastouri P, Prsa MJ, Ottensmeyer M, Akaishi S, Orgill DP, Ogawa R. Analysis of neuropeptides in stretched skin. Plast Reconstr Surg. 2009; 124(1):102–13. [PubMed: 19568049]
15. Daya M, Nair V. Traction-assisted dermatogenesis by serial intermittent skin tape application. Plast Reconstr Surg. 2008; 122(4):1047–54. [PubMed: 18827635]
16. Holle G, Germann G, Sauerbier M, Riedel K, von Gregory H, Pelzer M. Vacuum-assisted closure therapy and wound coverage in soft tissue injury. Clinical use. Unfallchirurg. 2007; 110(4):289–300. [PubMed: 17404700]
17. Orgill DP, Manders EK, Sumpio BE, Lee RC, Attinger CE, Gurtner GC, Ehrlich HP. The mechanisms of action of vacuum assisted closure: more to learn. Surgery. 2009; 146(1):40–51. [PubMed: 19541009]
18. McNulty AK, Schmidt M, Feeley T, Kieswetter K. Effects of negative pressure wound therapy on fibroblast viability, chemotactic signaling, and proliferation in a provisional wound (fibrin) matrix. Wound Repair Regen. 2007; 15(6):838–46. [PubMed: 18028132]
19. Pietramaggiori G, Liu P, Scherer SS, Kaipainen A, Prsa MJ, Mayer H, Newalder J, Alperovich M, Mentzer SJ, Konerding MA, et al. Tensile forces stimulate vascular remodeling and epidermal cell proliferation in living skin. Ann Surg. 2007; 246(5):896–902. [PubMed: 17968184]
20. Saxena V, Hwang CW, Huang S, Eichbaum Q, Ingber D, Orgill DP. Vacuum-assisted closure: microdeformations of wounds and cell proliferation. Plast Reconstr Surg. 2004; 114(5):1086–96. discussion 1097–8. [PubMed: 15457017]
21. Greene AK, Puder M, Roy R, Arsenault D, Kwei S, Moses MA, Orgill DP. Microdeformational wound therapy: effects on angiogenesis and matrix metalloproteinases in chronic wounds of 3 debilitated patients. Ann Plast Surg. 2006; 56(4):418–22. [PubMed: 16557076]

22. Scherer SS, Pietramaggiori G, Mathews JC, Prsa MJ, Huang S, Orgill DP. The mechanism of action of the vacuum-assisted closure device. Plast Reconstr Surg. 2008; 122(3):786–97. [PubMed: 18766042]

23. Morykwas MJ, Simpson J, Punger K, Argenta A, Kremers L, Argenta J. Vacuum-assisted closure: state of basic research and physiologic foundation. Plast Reconstr Surg. 2006; 117(7 Suppl):121S–126S. [PubMed: 16799379]

24. Morykwas MJ, Argenta LC, Shelton-Brown EI, McGuirt W. Vacuum-assisted closure: a new method for wound control and treatment: animal studies and basic foundation. Ann Plast Surg. 1997; 38(6):553–62. [PubMed: 9188970]

25. Wikswo JP, Prokop A, Baudenbacher F, Cliffel D, Csukas B, Velkovsky M. Engineering challenges of BioNEMS: the integration of microfluidics, micro- and nanodevices, models and external control for systems biology. IEE Proc Nanobiotechnol. 2006; 153(4):81–101. [PubMed: 16948492]

26. Helmke BP, Minerick AR. Designing a nano-interface in a microfluidic chip to probe living cells: challenges and perspectives. Proc Natl Acad Sci U S A. 2006; 103(17):6419–24. [PubMed: 16618928]

27. Jeon NL. BioMEMS: forging new collaborations between biologists and engineers. J Vis Exp. 2007; (9):411. [PubMed: 18989451]

28. Kartalov EP, Walker C, Taylor CR, Anderson WF, Scherer A. Microfluidic vias enable nested bioarrays and autoregulatory devices in Newtonian fluids. Proc Natl Acad Sci U S A. 2006; 103(33):12280–4. [PubMed: 16888040]

29. Piccin E, Coltro WK, Fracassi da Silva JA, Neto SC, Mazo LH, Carrilho E. Polyurethane from biosource as a new material for fabrication of microfluidic devices by rapid prototyping. J Chromatogr A. 2007; 1173(1–2):151–8. [PubMed: 17964580]

30. Kuncova-Kallio J, Kallio PJ. PDMS and its suitability for analytical microfluidic devices. Conf Proc IEEE Eng Med Biol Soc. 2006; 1:2486–9. [PubMed: 17946118]

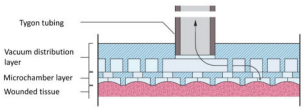

Figure 1.

Schematic representation of the two-layer microchamber array. The bottom layer comprises the microchamber that interface with the wound tissue. The upper layer comprises the vacuum distribution channel whereby the sub-atmospheric pressure is transmitted to the microchambers.

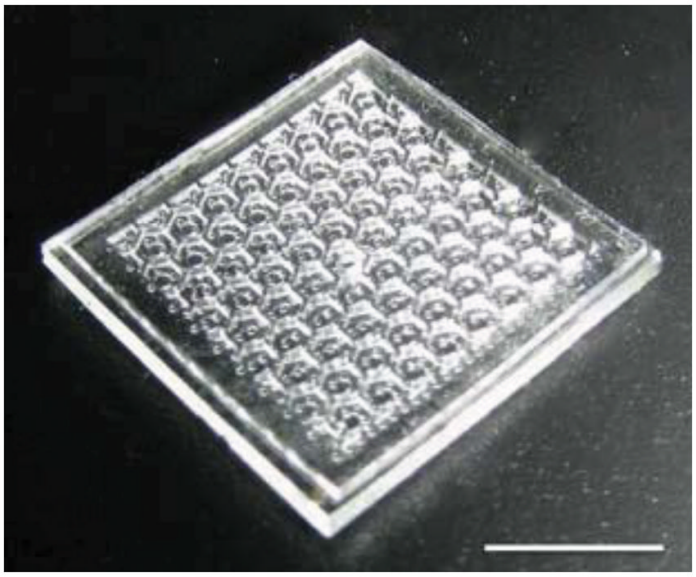

Figure 2.
Completed array dressing with microchamber diameter of 1000 μm and height of 200 μm. Bar = 4 mm.

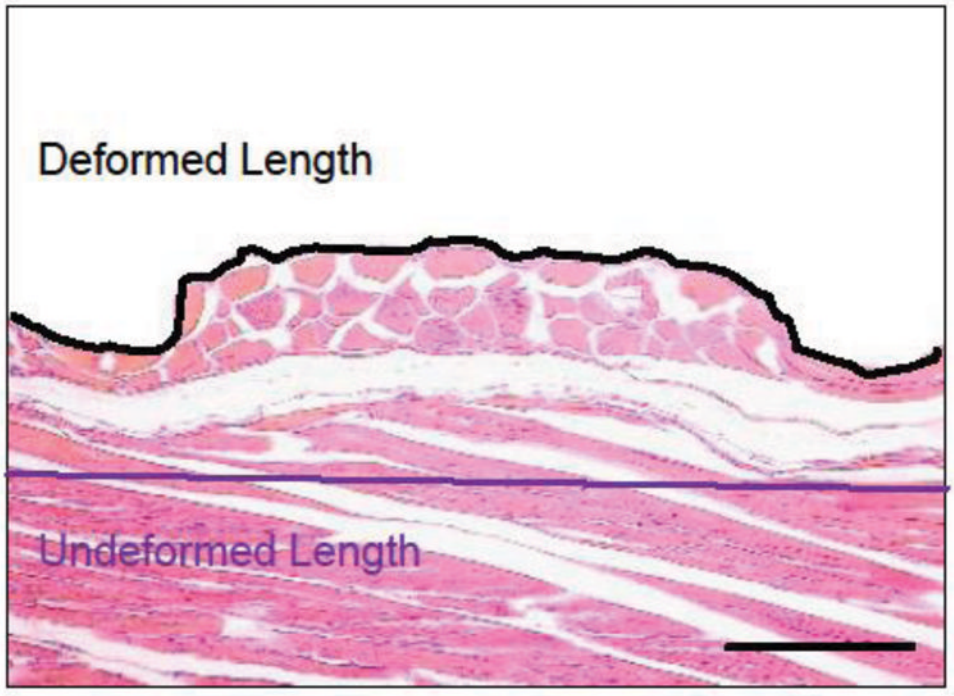

Figure 3.
Stained cross section of treated tissue including diagram of geometries used to determine tissue deformation. Deformation was found by dividing the length change by the undeformed length. Bar = 100 μm, 10x magnification.

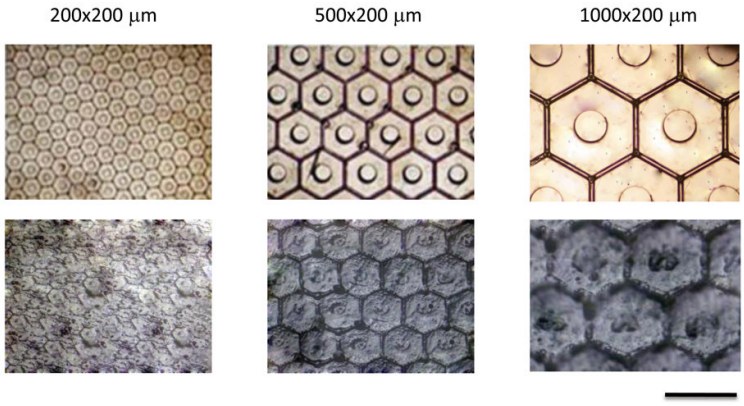

Figure 4.
Optical micrograph of microchambers and respective tissue deformations. Completed 200, 500, and 1000 μm wide (all 200 μm height) microchamber arrays at 4x magnification are shown in top panel. The bottom panel demonstrates wounded tissue deformation at 4x magnification following 12 hour application of μCAD under vacuum. Bar = 1000 μm.

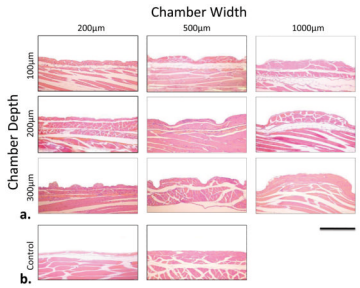

Figure 5.
Representative micrograph of sectioned and stained wound tissue following 12 hr application of μCAD device. Experimental groups results are shown in (a). Representative deformation from the negative control is shown on the left in (b) and the positive control results are shown on the right. Bar = 500 μm, 10x magnification.

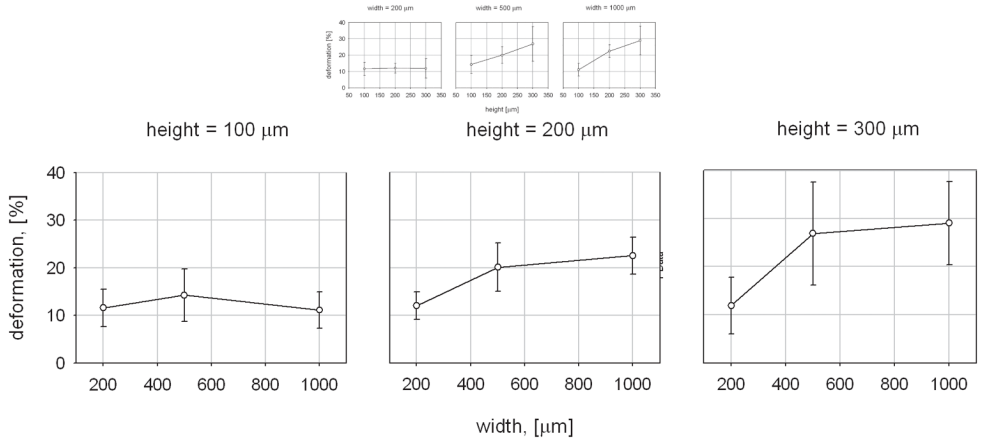

Figure 6.

Graphic representation of average tissue deformation for each microchamber size. Deformation as a function of height for each of the microchamber widths is shown in (a). Deformation as a function of width for each microchamber height is shown in (b).